arXiv:physics/0404053v2 [physics.optics] 2 Aug 2004

DENSITY EFFECTS IN FORWARD SCATTERING OF RESONANT LIGHT IN RUBIDIUM VAPOR

SZYMON PUSTELNY, WOJCIECH LEWOCZKO, WOJCIECH GAWLIK

Abstract. Transmission of light through an atomic sample placed between crossed polarizers in a magnetic field is jointly determined by Faraday rotation and net absorption: transmission increases with rotation and decreases with absorption. Both rotation and absorption are proportional to the atomic density N_0, hence, in a certain range of N_0, the two effects may compete yielding a distinct density dependence of the transmitted light. We have studied such dependence in rubidium vapor for $N_0 \approx 6.0 \times 10^9 \div 3.0 \times 10^{11}$ at/cm^3 with resonant laser light. We present interpretation of the competition effect and discuss its possible application for atomic density determination.

1. Introduction

Studies of magneto-optical effects in atoms and molecules have a long tradition. The advent of tunable lasers stimulated renewed interest in the nonlinear magneto-optics. Numerous papers are describing various aspects of this nonlinearity (see reference[1] for recent review). In the systems with ground state (or other long-lived lower levels) of angular momentum $J \neq 0$, the magneto-optical nonlinearities are due to optical pumping and Zeeman coherences. Optical pumping changes the saturation conditions for a given transition by affecting the sublevel populations whereas the Zeeman coherence allows interference of quantum paths linking different sublevels. These effects give rise to an optical anisotropy which can be easily studied experimentally.

One important application of magneto-optical studies is the determination of optical density and thus a measurement of oscillator strength (dipole moment) of a given transition when the number density is known or, inversely, of atomic densities when the transition probability is known. Examples of such applications of linear Faraday effect are the measurements of relative oscillator strengths in neon [2] and sodium [3] and of atomic vapor density of optically thick potassium vapors [4].

The present work describes experimental and theoretical analysis of transmission of resonance laser light by atomic vapors positioned between crossed polarizers in a weak longitudinal magnetic field (forward scattering - FS) under conditions of nonlinear light-matter interaction. In general, the FS signal, i.e. the transmitted light intensity vs. magnetic field, depends on the polarization anisotropy both in atomic absorption and dispersion. In such context FS has been analyzed for conventional light sources in early works of G. W. Series and coworkers [5], and for laser light by W. Gawlik et al.[6]. For a medium of length L, placed between crossed polarizers and characterized by refractive indices $n_\pm$ and absorption coefficients $\kappa_\pm$ for the $\sigma^\pm$ polarized light, the intensity of the forward-scattered monochromatic

light of wavenumber k is given by[3]

$$I_{FS} = \frac{I_0}{4}[e^{-\kappa_+ kL} - e^{-\kappa_- kL}]^2 + I_0 \sin^2[\frac{n_+ - n_-}{2} kL] e^{-(\kappa_+ + \kappa_-)kL}, \tag{1.1}$$

where I_0 is the incident light intensity. The FS signal is non-zero only if the medium possesses some optical anisotropy between the σ^+ and σ^- light polarizations. An important cause of such anisotropy is a longitudinal magnetic field which splits the $n_\pm(\omega)$ and $\kappa_\pm(\omega)$ profiles. The first part of Eq. (1.1) describes the effect of medium dichroism whereas the second part is due to its birefringence weighted by a net absorption. For the light frequency ω tuned exactly to the atomic transition frequency ω_0 and for a linear splitting of atomic energy levels due to magnetic field, the appearance of a nonzero FS signal is caused exclusively by the second part of expression (1.1), i.e. by the birefringence. The exact shape of the FS signal dependence on the magnetic field is affected by a combined effect of birefringence and total absorption. In the case of nonlinear interaction with the light beam, this dependence may have the form of a narrow sub-Doppler, or even subnatural, resonances (see, e.g. references [1, 6]). The two properties of the medium, birefringence and total absorption, scale differently with the atomic density which results in specific density/temperature characteristics of the FS signals discussed below. We hope that these characteristic density dependences would be useful for determination of the optical density of atomic samples.

The detailed mechanism of nonlinear FS signals has been theoretically analyzed in several papers (see, e.g. references[7, 8, 9, 10, 11, 12]) at different levels of accuracy. Below, we present a nonperturbative treatment that for low J values yields analytical formulae.

In the next section we describe our setup and present experimental results. In Sec. 3 we present theoretical calculations and interpretation of the experiment. Finally, we conclude in Sec. 4.

2. Experiment

2.1. **Apparatus.** The experimental setup is shown in Fig. 1. We used an external cavity diode laser tuned to the hfs component $F_g = 3 \rightarrow F_e = 2$ of the ^{85}Rb D_1 line. The laser frequency was stabilized by an external stabilization system based on Doppler-free dichroism[13]. The light beam of 2 mm diameter was linearly polarized and its power was varied by rotation of a $\lambda/2$-waveplate in the range 0 to 4 mW. The laser light was passing through a 5 cm long cylindrical glass cell of 2 cm diameter filled with the natural mixture of ^{85}Rb and ^{87}Rb and no buffer gas. The cell was heated by a nonmagnetic heater to temperatures between 20 ^{o}C and 60 ^{o}C which yielded saturated vapors with densities in the range $6.0 \times 10^9 \div 3.0 \times 10^{11}$ at/cm^3. A pair of Helmholtz coils produced the longitudinal magnetic field of -3 G to 3 G value. The cell and the coil system were surrounded by a three-layer magnetic shield made of mu-metal. As assessed from the resonance line-width, the shielding efficiency was better than 10^4. Polarizer P and crossed analyzer A were mounted outside the shield[5]. In that geometry, detector D placed behind the analyzer registered only the FS signal due to rotation of the polarization plane of the transmitted light and/or its ellipticity. Part of the incident beam was directed to the saturation spectroscopy system which served as frequency reference.

2.2. **Results.** The FS signals, $I_{FS}(B)$, were recorded as a function of the magnetic field B for various temperatures T and light intensities I_0. The narrowest features in signals are caused by nonlinear Faraday effect due to ground-state optical pumping and Zeeman coherences. A typical plot of that part of the FS signal is presented in Fig. 2a. The amplitude of the signal, defined as A_{FS} in Fig. 2a, depends on the light intensity and concentration of the atomic vapors. In Fig. 3 we summarize the results of the amplitude vs. temperature T dependences taken for various light intensities I_0.

For the studied range of intensities between 1 mW/cm^2 and 6 mW/cm^2, the signals exhibit characteristic temperature dependence: for low temperature their amplitudes increase with T then reach their maxima and subsequently decrease with T. The temperature of the maximum amplitude shifts with the light intensity. For high temperatures almost no light is transmitted through the cell between crossed polarizers. For very high light intensity (above 100 mW/cm^2), the maximum shifts even beyond the range of temperatures available with our setup (Fig. 4).

We have verified that the amplitude of the FS signal is a nonlinear function of the light intensity. This could be expected as the intensities we were using were close to, or higher than, the saturation intensity which for rubidium is 1.6 mW/cm^2. It can be thus expected that the interplay between rotation and absorption is affected by different saturation behavior of the dispersive and absorptive atomic properties. Such different saturation effects are manifest in Fig. 3 by a shift of the maxima towards higher temperatures with increasing I_0.

3. Interpretation

The properties of the maxima in the $A_{FS}(T)$ dependences, described above, are independent of the detailed mechanisms responsible for the FS signals. The maximum occurs for linear, as well as for nonlinear Faraday rotations. For nonlinear Faraday effect, it appears no matter if the FS signals have natural or sub-natural widths, i.e. if they are due to population redistribution or Zeeman coherences. The detailed nature of atomic birefringence and absorption mechanism affects only the range of the concentrations (temperatures) where the maximum is visible.

This property can be illustrated by the following simple arguments. For exact resonance, $\delta = 0$, only the second part of Eq.(1.1) differs from zero, hence

$$\frac{I_{FS}}{I_0} = \sin^2(\alpha N_0)\exp(-\beta N_0), \tag{3.1}$$

where $\alpha/\beta = 1/2(n_+ - n_-)/(\kappa_+ + \kappa_-)$ and N_0 is the atomic concentration. For a given atomic transition, cell length, magnetic field and light intensities, α and β are constants mutually related by the Kramers-Kronig relation [14]. I_{FS}/I_0 is thus an universal function of N_0, parameterized by the ratio α/β but *independent of the detailed form* of α and β. Generally, the specific value of the ratio depends on particular dependences of α and β on atomic energy level structure, mechanism of interaction with the external fields and their intensities. However, for the value of the magnetic field corresponding to maximum rotation A_{FS} the splitting of atomic magnetic sublevels is nearly equal to their width which results in α/β of the order of 1. By virtue of the Kramers-Kronig relation, the value of α/β at a given B is nearly insensitive to the details of the atomic structure and to the nature of optical anisotropy. With $\alpha/\beta = 1$, expression (3.1) represents a strongly damped oscillatory dependence on N_0, dominated by the first oscillation. These

oscillations are nonlinear counterparts of those described in reference [3]. Note, that the appearance of the characteristic maximum of the A_{FS} dependence on N_0 is possible only with the FS methodology and cannot be observed by measuring only the rotation.

For more quantitative interpretation of our experimental results we use semiclassical approach of forward scattering and density matrix formalism[15] to calculate the refractive indices n and absorption coefficients κ

$$n - 1 = \frac{\Re(\sum_i d_i \langle \rho_{coh}^{(i)} \rangle_v)}{E\epsilon_0}, \tag{2a}$$

$$\kappa = \frac{\Im(\sum_i d_i \langle \rho_{coh}^{(i)} \rangle_v)}{E\epsilon_0}, \tag{2b}$$

where $\langle \rho_{coh}^{(i)} \rangle_v$ are the velocity averaged optical coherences for the i-th transition of a given polarization, $\Re$ and $\Im$ denote their real and imaginary parts, respectively, d_i is the dipole moment of the particular transition, E the amplitude of the light electric field, and ϵ_0 is the electric permittivity of free space.

In this paper we consider the simple model of atomic structure $J_g = 1/2 \rightarrow J_e = 1/2$ with two sublevels in the ground state and two sublevels in the excited state the, so called, X model. The σ^+ component of the propagating beam excites atoms from the ground-state sublevel $|a\rangle$ ($m = -1/2$) to the excited-state sublevel $|B\rangle$ ($m = 1/2$). Analogically, the σ^- component causes transition from $|b\rangle$ ($m = 1/2$) to $|A\rangle$ ($m = -1/2$). The great advantage of this simple model is its analytical solvability. Despite its simplicity, the X model gives good qualitative agreement with the experimental results. Furthermore it reproduces well the observed dependence of the FS amplitude on the properties of the atomic medium, in particular on the dipole moment and concentration of atoms in the ground sublevels in thermal equilibrium.

To check to what extent the density dependence of $A_{FS}(N_0)$ is insensitive to particular model, and to verify that the X model does not oversimplify the interpretation, we have additionally applied another model using the Λ-type atomic structure (Fig. 5b). The second model allows proper analysis of the coherence effects, such as coherent population trapping (CPT) [16], and their consequences for magneto-optical properties of the medium. However, analytical solutions and velocity integration are much more difficult within the second model. For this reason, in this paper we concentrate exclusively on the X model. Nevertheless, we have verified by numerical calculation with the Λ model that Zeeman coherence effects do not change qualitative predictions of the X model concerning the temperature dependence of $A_FS(N)$. This is due to the fact that the $I_FS(B)$ signals simulated by both models are qualitatively very similar to the experimental ones, as seen in Fig.2, so the α and β quantities in Eq. (2) remain very close, no matter what detailed model is being used.

Within our model, the refractive indices and absorption coefficients for both circular polarizations are calculated using equations (2a) and (2b) as

$$n_+ - 1 = \frac{d\Re(\langle \rho_{aB} \rangle_v)}{E\epsilon_0},\ n_- - 1 = \frac{d\Re(\langle \rho_{bA} \rangle_v)}{E\epsilon_0}, \tag{3a}$$

(3b) $$\kappa_+ = \frac{d\Im(\langle\rho_{aB}\rangle_v)}{E\epsilon_0},\ \kappa_- = \frac{d\Im(\langle\rho_{bA}\rangle_v)}{E\epsilon_0}\ .$$

The semiclassical Hamiltonian of the system is given by

(4)
$$H = \hbar\omega_0(\rho_{AA}+\rho_{BB})+\frac{\hbar}{2}g_g\omega_B(\rho_{aa}-\rho_{bb})+\frac{\hbar}{2}g_e\omega_B(\rho_{AA}-\rho_{BB})+dE(\rho_{aB}+\rho_{bA}+h.c.),$$

where ρ_{ii} denotes population of the i-th state, g_g, g_e are the Landé factors of the ground and the excited states, respectively, ω_0 is the transition frequency in zero magnetic field, and ω_B is the Larmor frequency $\omega_B = \mu_B B/\hbar$ with μ_B being Bohr magneton.

Evolution of the density matrix is described by the master equation

(5) $$\dot{\rho} = -\frac{i}{\hbar}[H,\rho] - \tilde{\Gamma}\rho,$$

where $\tilde{\Gamma}\rho$ stands for the relaxation operator.

Formula (5) yields the following equations describing evolution of the optical coherences in the X model

(6a) $$\dot{\rho}_{aB} = i(\omega_0 + \omega'_B + i\Gamma)\rho_{aB} + i\beta(\rho_{aa} - \rho_{BB}),$$

(6b) $$\dot{\rho}_{bA} = i(\omega_0 - \omega'_B + i\Gamma)\rho_{bA} + i\beta(\rho_{bb} - \rho_{AA}),$$

where $\omega'_B = \frac{1}{2}(g_g+g_e)\,\omega_B$ is the effective magnetic shift of the resonance frequency, $\beta = Ed/\hbar$ is the Rabi frequency and Γ is the relaxation constant of the optical coherences.

Further calculations are performed in the rotating-wave and steady state approximations. Under such conditions the optical coherences become

(7a) $$\tilde{\rho}_{aB} = -\frac{\beta}{\delta + \omega'_B + i\Gamma}(\rho_{aa} - \rho_{BB}),$$

(7b) $$\tilde{\rho}_{bA} = -\frac{\beta}{\delta - \omega'_B + i\Gamma}(\rho_{bb} - \rho_{AA}),$$

where $\tilde{\rho}_{aB}$ and $\tilde{\rho}_{bA}$ are slowly-varying coherences in the rotating-wave approximation and $\delta = \omega_0 - \omega$. Although only $\tilde{\rho}_{aB}$ is calculated below, the analogical calculation can be performed for $\tilde{\rho}_{Ba}$.

Relation (7a) couples the optical coherence with atomic populations. Using Eq. (5) to calculate atomic populations and inserting them to (7a) one can write

(8) $$\tilde{\rho}_{aB} = \beta n_{eq}(\delta + \omega'_B - i\Gamma)\frac{M_A(\delta) + 2rG}{M_A(\delta)M_B(\delta) + rG(M_A(\delta) + M_B(\delta)) + 2rG^2},$$

where n_{eq} is the thermal equilibrium atomic population of the ground state and other symbols are defined as

$$M_A(\delta) = (\delta - \omega'_B)^2 + \Gamma^2,$$
$$M_B(\delta) = (\delta + \omega'_B)^2 + \Gamma^2,$$
$$r = \frac{\gamma_e}{3\gamma_g},$$

$$G = \frac{2\beta^2\Gamma}{\gamma_e},$$

with γ_g and γ_e being the relaxation constants of the ground and excited states, respectively. Relation (8) is an analitical expression valid for any light intensities and allowing easy analysis of the dispersive and absorptive responses of our model system to light and magnetic field. Perturbative solutions for optical coherences can be obtained in the low light power regime, $G \ll 1$, by expanding relation (8) into power series of G.

Relation (8) contains the ratio of two polynomials of δ (they also depend on ω'_B). At this point atomic movement needs to be taken into consideration, i.e. δ has to be corrected for Doppler shifts ($\delta \to \delta - kv$) and expression (8) needs to be integrated over the Maxwell distribution of the velocities v. Generally, this is the place when one sacrifices analyticity of solutions for a single velocity class. However, the benefits of analytic expressions can be retained by expanding (8) into partial fractions

$$\tilde{\rho}_{aB} = -n_{eq}\beta[\frac{A_+(\omega'_B)}{\delta + \delta_1(\omega'_B)} + \frac{A_-(\omega'_B)}{\delta - \delta_1(\omega'_B)} + \frac{B_+(\omega'_B)}{\delta + \delta_2(\omega'_B)} + \frac{B_-(\omega'_B)}{\delta - \delta_2(\omega'_B)}], \tag{9}$$

where $\delta^2_{1,2} = B^2 - \gamma^2 - rG \pm \sqrt{r^2G^2 - 4B^2(\gamma^2 + rG) - 2rG^2}$ are the roots of the denominator of Eq. (8), while $A_\pm$, $B_\pm$ are the expansion coefficients equal to

$$A_\pm = \frac{1}{2}\frac{\delta_1^3 \mp a\delta_1^2 + b\delta_1 \mp c}{\delta_1(\delta_1^2 - \delta_2^2)}, \quad B_\pm = -\frac{1}{2}\frac{\delta_2^3 \mp a\delta_2^2 + b\delta_2 \mp c}{\delta_2(\delta_1^2 - \delta_2^2)},$$

where $a = B + i\gamma$, $b = 2rG - (a^*)^2$, and $c = -a^*(2rG + |a|^2)$. One thus obtains

$$\begin{aligned}\langle\tilde{\rho}_{aB}\rangle_v = -\frac{n_{eq}\beta N_0}{\sqrt{\pi}u}[&A_+(\omega'_B)\int_{-\infty}^{\infty}\frac{\exp(-v^2/u^2)\,dv}{\delta - kv + \delta_1(\omega'_B)} \\ &+A_-(\omega'_B)\int_{-\infty}^{\infty}\frac{\exp(-v^2/u^2)\,dv}{\delta - kv - \delta_1(\omega'_B)} \\ &+B_+(\omega'_B)\int_{-\infty}^{\infty}\frac{\exp(-v^2/u^2)\,dv}{\delta - kv + \delta_2(\omega'_B)} \\ &+B_-(\omega'_B)\int_{-\infty}^{\infty}\frac{\exp(-v^2/u^2)\,dv}{\delta - kv - \delta_2(\omega'_B)}],\end{aligned} \tag{10}$$

where u is the average atomic speed. Writing down the coherence in form (10) allows a clear interpretation of each contribution. The functions $A_\pm(\omega'_B)$, $B_\pm(\omega'_B)$ are responsible for narrow structures in the FS signals and describe the nonlinear Faraday effect, while the integrals describe wide pedestals of $I_{FS}(\omega'_B)$, barely visible in a narrow scan of the magnetic field. For calculations of the integrals in (10), standard tabularized functions, the plasma dispersion function [17] or the complex error function [18], can be used.

As it was mentioned above, the FS signal registered with the crossed polarizers arrangement results from competition between rotation of the polarization plane and net absorption. The competition is seen in Eq.(1.1) which for $\delta = 0$, takes the form

$$I_{FS} = I_0 \sin^2(\frac{n_+ - n_-}{2}kL)\exp(-2\kappa kL), \tag{11}$$

where $\kappa = \kappa_+(\omega_B, \delta = 0) = \kappa_-(\omega_B, \delta = 0)$. Relation (10) was used for simulation of the FS signals with parameters corresponding to the experimental conditions:

$d = 2.25 \times 10^{-29}$ Cm, $u = 200$ m/s, $g_e = g_g = 1$, $\gamma_g = 2\pi \times 0.1$ MHz, $\gamma_e = 2\pi \times 5.74$ MHz, and $\Gamma = 2\pi \times 2.92$ MHz. The ground-state relaxation rate γ_g reflects finite atomic transit time across the laser beam. In the D_1 line of rubidium, there are two transitions within the Doppler width that can be excited by light: $F_g = 3 \rightarrow F_e = 2$ and $F_g = 3 \rightarrow F_e = 3$ but since in our experiment the laser was tuned only to the $F_g = 3 \rightarrow F_e = 2$ component, the contribution of another transition has been neglected. Apart from a very simplified atomic structure, the present analysis also does not take into account specific relaxation mechanisms, e.g. velocity-changing collisions[19] and/or radiation trapping [20] which may affect the specific ratio α/β in Eq. (3.1).

Results of the simulations with our X model of the FS signal amplitude vs. atomic concentration are shown in Fig. 6 for various light intensities.

As the experimental results were recorded vs. vapor temperature, the atomic density in Eq. (10) has to be expressed as a function of the vapor temperature which is possible if the temperature dependence of rubidium vapor pressure is known. The issue of vapor pressure is crucial for many experimental situations, yet exact measurements of vapor pressures are difficult and subject to various systematic errors. A common procedure is to use one of the existing compilations which fit experimental data obtained in various temperatures by simple analytical formulae that can be used for extra- or interpolation to other temperatures. In principal, such fits are based on the statistical physics and chemistry laws (Arrhenius law, ideal gas law) with possible corrections for departures from the ideal gas model and/or for specific metal evaporation conditions. Particular care should be taken close to phase-transition temperatures, as e.g. near the melting point. This is the case of our experimental conditions as the melting point of rubidium 39.3 ^{o}C occurs just in the middle of our temperature range.

Assuming ideal gas and starting from the Arrhenius relation, the saturated vapor pressure could be determined by formula

$$\log_{10} p(T) = A - \frac{B}{T}. \tag{12}$$

Such a dependence is used, e.g. in reference[21], which for rubidium gives $A = 4.875$ and $B = -4215$ below the melting point and $A = 4.312$ and $B = -4040$ above the melting temperature. Another widely cited compilation [22] applies extra corrections terms and uses relation

$$\log_{10} p(T) = A' + \frac{B'}{T} + C'T + D' \log_{10} T, \tag{13}$$

where for rubidium $A' = 94.05$, $B' = 1961$, $C' = -0.03772$, and $D' = 42.57$ below the melting temperature and $A' = 15.88$, $B' = 4330$, $C' = 0.00059$, and $D' = -2.99$ above the melting point. From Eqs. (12) and (13), with the help of ideal gas equation, $pV = N_{at} k_B T$ (N_{at} is the number of atoms the gas, V is its volume, and k_B the Boltzmann constant), one can obtain the final concentration-temperature relation $N_0(T)$. Reliability of such density determination depends obviously on quality of experimental data used for a given analytic fit. Reference[23] presents a thorough comparison of several measurements of rubidium vapor pressure vs. temperature which appears to be fairly consistent with the Nesmeyanov's prediction[22]. On the other hand, the CRC compilation[21] is based on not too many experiments and, to our best knowledge, has not been verified in a wide range of temperatures.

Our experiment interpreted in terms of the X model yields for $T \approx 50$ ^{o}C the density that is consistent with the data given by[21] and by 25% higher from the value given in reference[22]. We hope that after more detailed interpretation, the described method could allow accurate measurements of the atomic vapor densities and possibly improve existing literature inconsistencies.

Comparison of Fig. 3 with Fig. 7 shows that while there is not a perfect agreement of the simulated signals with the experimental ones, they are very similar and exhibit the same general character. For low temperatures the FS amplitude scales as a square function of the concentration N_0. This part of the dependences is determined only by the dispersive properties of the medium. For higher temperatures the absorption starts to play an important role and cannot be neglected anymore. The interplay between dispersion and absorption produces the maximum of the FS amplitude signal. For even higher temperatures, the absorption of the transmitted light becomes dominant and the amplitudes of the FS signals decrease exponentially with concentration N_0. In addition to this temperature/density dependence, the FS amplitude rises and shifts with increase of the incident light intensity. The shifts of the maxima positions for various light intensities are due to different saturation behavior of the dispersion and absorption coefficients which affects the α/β ratio in Eq. (3.1). This is a very interesting effect that deserves independent systematic study, preferably with more complex models of atomic structure.

4. Conclusions

The specific effect of competition between polarization rotation and absorption, described above, shows up in the FS signals. The FS intensity, given by Eq. (10), increases with the medium birefringence (as $\sin^2$ of the Faraday angle) and decreases exponentially with the medium absorption. Competition of these opposite trends is responsible for the observed maxima of the dependences seen in Figs. 3 and 7. Appearance of this competition is an universal feature, independent of whether the light-matter interaction has a linear or a nonlinear character. The possible nonlinearity only affects the absolute scale of the rotation and absorption and, consequently, the range of densities where the competition occurs. For alkali metal vapors and for light intensities of the order of 1 mW/cm^2, the resonant nonlinear Faraday effect allows observation of such a competition already in a low-density range, about $N_0 \approx 10^{10}$ at/cm^3, which requires temperatures not much higher than the room temperature. The onset of optical nonlinearity not only lowers the density at which the characteristic maximum of the $A_{FS}(N_0)$ dependence appears but results in its shift with the light intensity. This is due to different saturation behavior of the dispersive and absorptive atomic properties.

We note that the main features of the discussed dependences do not depend on the detailed mechanism of the nonlinearity. We have considered two physically different models in which the nonlinearities are caused by two different mechanisms: either they are due to redistribution of populations between Zeeman sublevels (optical pumping), or are due to the coherence established between the sublevels. Both models gave very similar results and reproduced our experimental observations. The very distinct result of the competition between absorption and rotation, i.e. the maximum of the forward scattering amplitude signal, appears at well determined value of the atomic density. We believe that existence of such characteristic point whose position is well defined function of the atomic properties of the medium and

scattered light intensity should allow precise determination of the atomic number densities or transition probabilities.

5. Acknowledgements

We acknowledge stimulating and helpful discussions with Dmitry Budker, Krzysztof Sacha and Jerzy Zachorowski whose experimental help is also very appreciated. This work was partially supported by NRC U.S.-Poland Twinning Grant No.015369, and by the Polish KBN grant No. 3T11B 079 26. It was also a part of a program of Polish National Laboratory of AMO Physics in Toruń, Poland (grant No. PBZ/KBN/043/PO3/2001).

References

1. D. Budker, W. Gawlik, D. F. Kimball, S. M. Rochester, A. Weis, and V. V. Yashchuk, "Resonant nonlinear magneto-optical effects in atoms", Rev. Mod. Phys. **74**, 1153-1201 (2002).
2. W. Seka and F.L. Curzon, "Measurements of relative transition probabilities using Faraday effect", J. Quant. Radiat. Transfer **8**, 1147-1162 (1968).
3. W. Gawlik, J. Kowalski, R. Neumann, and H. B. Wiegemann, "A new method for measuring oscillator strengths using the resonant Faraday effect in monochromatic light", J. Phys. B (At. Mol. Phys.) **12**, 3873-3882 (1979).
4. E. Vliegen, S. Kadlecek, L. W. Anderson, T. G. Walker, C. J. Erickson, and W. Happer, "Faraday rotation density measurements of optically thick alkali metal vapors", Nucl. Instr. Meth. A **460**, 444-450 (2001).
5. A. Corney, B. P. Kibble, and G. W. Series, "Forward scattering of resonance radiation with special reference to double resonance and level-crossing experiments", Proc. R. Soc. London, Ser. A **293**, 70-93 (1966).
6. W. Gawlik, J. Kowalski, and R. Neumann, F. Träger, "Observation of the electric hexadecapole moment of free Na atoms in a forward scattering experiment", Opt. Commun. **12**, 400-404 (1974).
7. S. Giraud-Cotton, V. P. Kaftandjian, and L. Klein, "Forward scattering of resonant radiation as a function of applied magnetic field theoretical study of the hyperfine lines of the sodium doublet", Phys. Lett. A **88**, 453-436 (1982).
8. X. Chen, V. L. Telegdi, and A. Weis, "Quantitative study of the nonlinear Macaluso-Corbino (resonant Faraday) effect in Cs", Opt. Commun. **74**, 301-305 (1990).
9. B. Ståhlberg, P. Jungner, T. Fellman, and A. Lindberg, "Nonlinear forward scattering of resonant laser-light from excited neon systems", Appl. Phys. B **50**, 547-551 (1990).
10. F. Schuller and D. N. Stacey, "Magneto-optical rotation in atomic transitions between levels with J=0 and J=1", Phys. Rev. A **60**, 973-981 (1999).
11. B. W. Holmes and J. A. R. Griffith, "A detailed study of the effects of weak magnetic fields on the forward scattering of resonant laser light by sodium vapour", J. Phys. B **28**, 2829-2846 (1995).
12. B. Łobodziński and W. Gawlik, "Multipole moments and trap states in forward scattering of resonance light", Phys. Rev. A **54**, 2238-2252 (1996).
13. G. Wąsik, W. Gawlik, J. Zachorowski, and W. Zawadzki, "Laser frequency stabilization by Doppler-free magnetic dichroism", Appl. Phys. B **75**, 613-619 (2002).
14. J. D. Jackson, *Classical Electrodynamics*, (Wiley, New York, 1972), Chapter 7.
15. R. W. Boyd *Nonlinear Optics* (Academic, Boston, 1992), Chapter 3.
16. E. Arimondo, "Coherent population trapping in laser spectroscopy", *Progress in Optics* **XXXV**, E. Wolf Ed., Elsevier, 1996, pp. 259-354.
17. B. Fried and S. Conte, *The Plasma Dispersion Function* (Academic Press, New York, 1961).
18. M. Abramovitz and I. A. Stegun, *Handbook of Mathematical Functions*, (Dover, New York, 1972), p. 297.
19. E. Arimondo, "Relaxation processes in coherent-population trapping", Phys. Rev. A **54**, 2216-2223 (1996).
20. A. B. Matsko, I. Novikova, M. O. Scully, and G. R. Welch, "Radiation Trapping in Coherent Media", Phys. Rev. Lett. **87**, 133601 (2001).

21. *CRC Handbook of chemistry and Physics, 73rd Edition*, D. R. Lide Ed., CRC Press, Boca Raton, 1992, p. 5-80.
22. A. N. Nesmyanov, *Vapor pressures of the chemical elements*, Elsevier, New York, 1963.
23. D. C. Thompson and G.-X. Xu, "Optical measurements of vapor pressures of Rb and a Rb-K mixture", Can. J. Phys. **60**, 1496-1501 (1982).

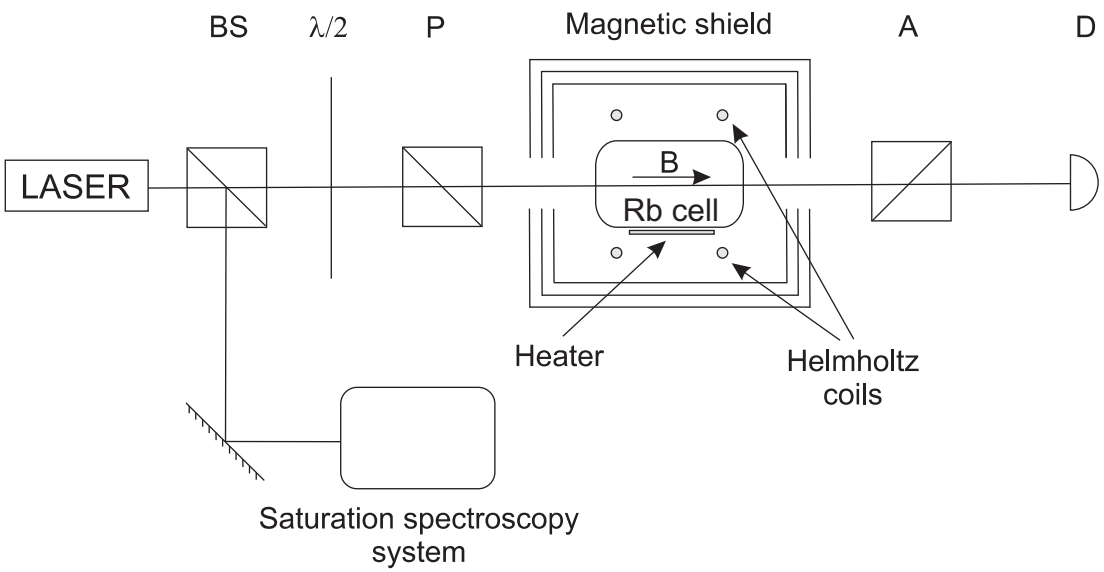

FIGURE 1. Experimental setup. BS is the beam-splitter, P, A are polarizer and analyzer, respectively, $\lambda/2$ is $\lambda/2$-waveplate and D is a photodetector.

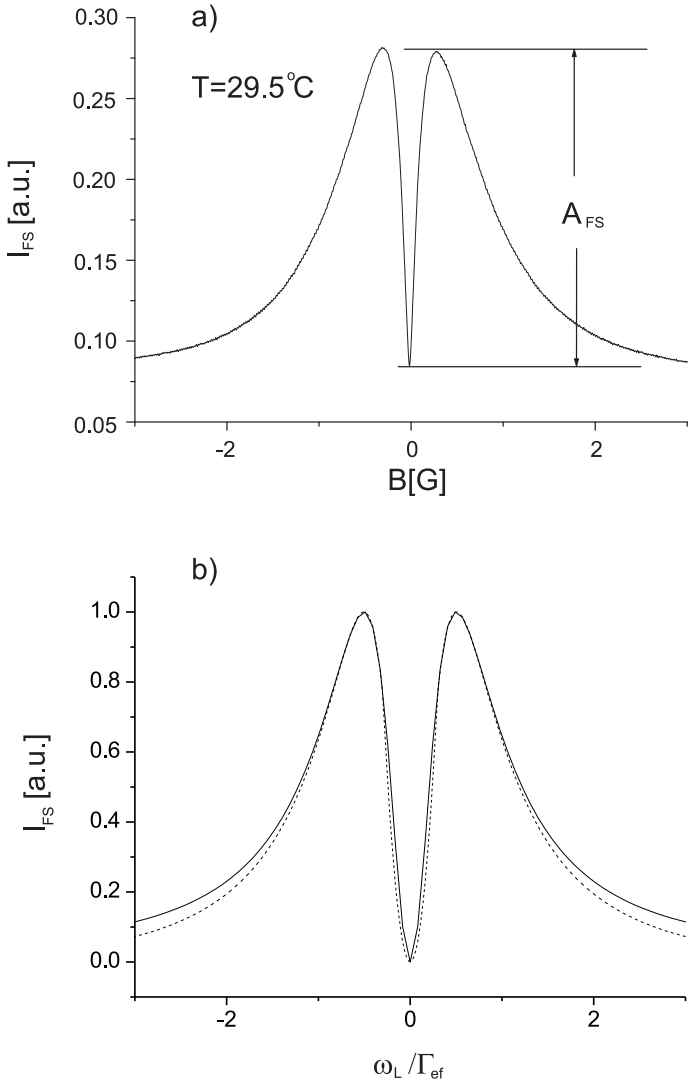

FIGURE 2. Typical forward scattering signal, $I_{FS}(B)$, recorded for cell temperature 29.5 ^{o}C and light intensity $I_0 = 2.2$ mW/cm^2 (a). FS signals calculated with the X model (solid line) and Λ model (dashed line) (b). A_{FS} denotes the amplitude of the FS signal. The theoretical signals correspond to incident light intensity $I_0 = 0.6$ mW/cm^2. They are presented in domain of Larmor frequency over effective width ($\Gamma_{ef} = \Gamma$ for the X model and $\Gamma_{ef} = \gamma_g$ for the Λ model) and are normalized to the same A_{FS}.

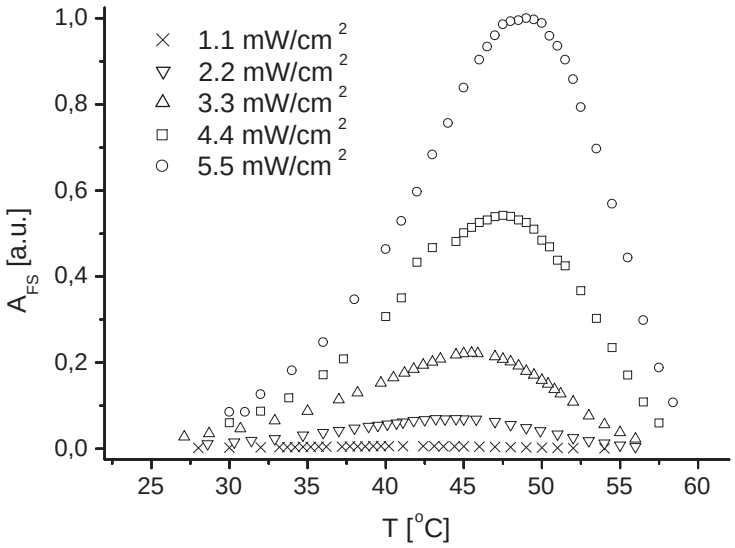

FIGURE 3. The amplitudes of the FS signals (A_{FS}) vs. temperature for various intensities of the incident light.

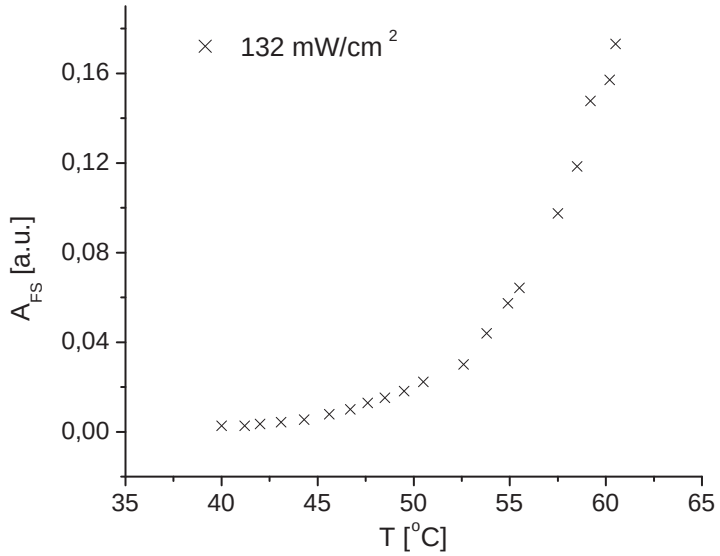

FIGURE 4. The amplitude of the FS signal (A_{FS}) vs. temperature for very high light intensity, $I_0 = 130$ mW/cm^2.

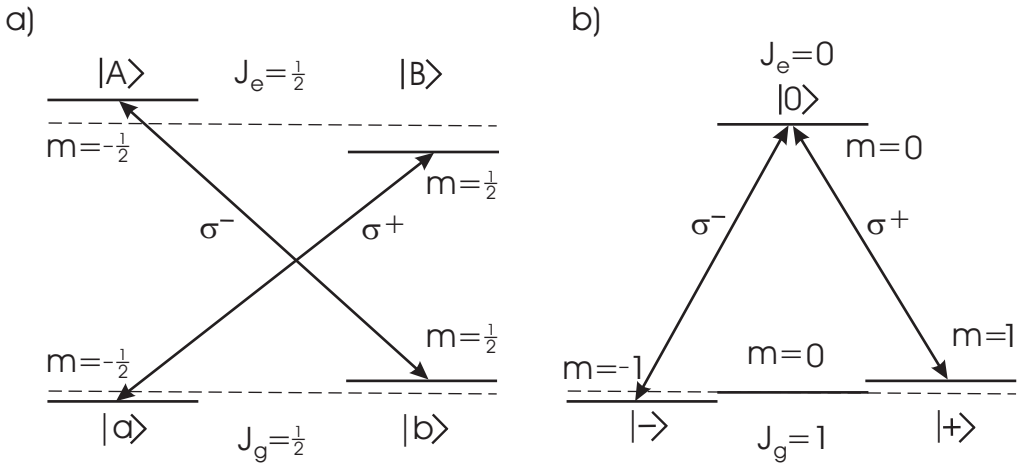

FIGURE 5. Energy level structure for a) the X-model, b) the Λ-model.

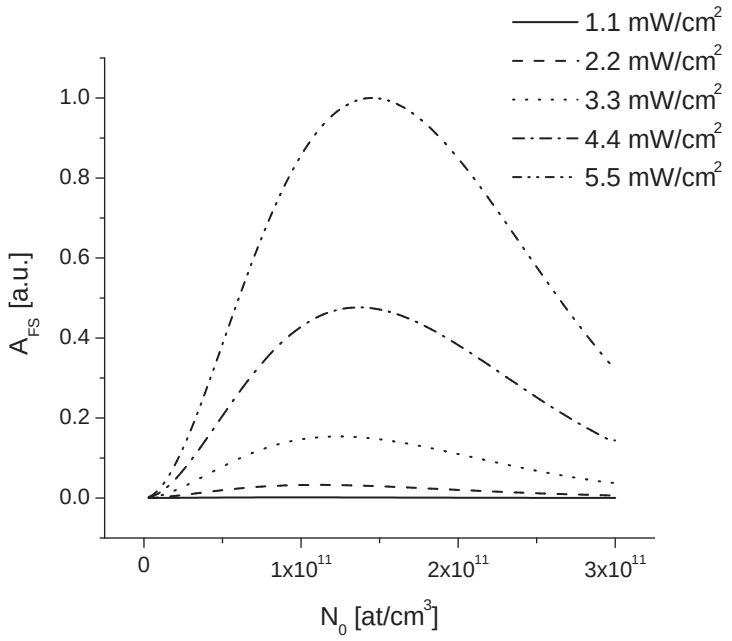

FIGURE 6. Results of numerical simulations of the FS signal amplitudes vs. atomic concentration for the same incident light intensities as used in experiment.

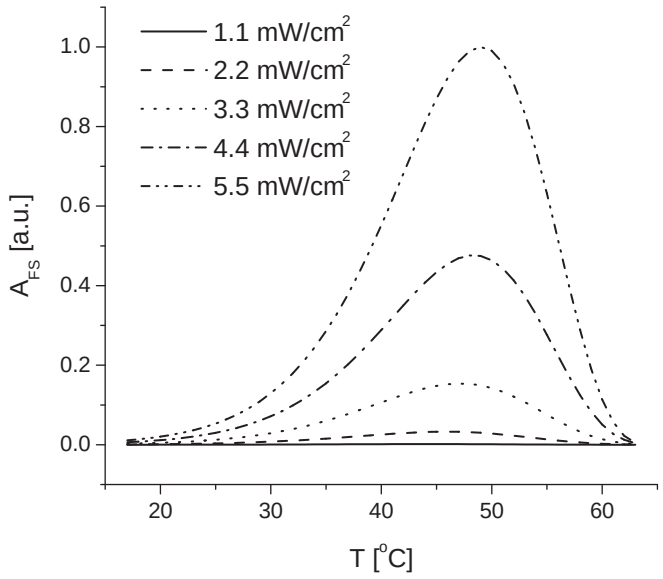

FIGURE 7. Results of numerical simulations of the FS signal amplitudes vs. vapor temperature for the light intensities as used in the experiment (compare with Fig. 3).

M. SMOLUCHOWSKI PHYSICAL INSTITUTE, JAGIELLONIAN UNIVERSITY, REYMONTA 4, 30-059 KRAKÓW, POLAND

E-mail address: pustelny@netmail.if.uj.edu.pl